




Stochastic currents and efficiency in an autonomous heat engine

Wenqi Lin , Yi-Hung Liao (廖宜鴻) , Pik-Yin Lai (黎璧賢) *, and Yonggun Jun (전용근) [†]

Department of Physics and Center for Complex Systems, National Central University, Taoyuan City 320, Taiwan



(Received 8 June 2022; accepted 10 August 2022; published 30 August 2022)

We experimentally demonstrate that a Brownian gyrotor of a colloidal particle confined in a two-dimensional harmonic potential with different effective temperatures on orthogonal axes can work as an autonomous heat engine capable of extracting work from the heat bath, generated by an optical feedback trap. The results confirm the theoretically predicted thermodynamic currents and validate the attainability of Carnot efficiency as well as the trade-off relation between power and efficiency. We further show that current fluctuations and the entropy production rate are time independent in the steady state and their product near the Carnot efficiency is close to the lower bound of the thermodynamic uncertainty relation.

DOI: [10.1103/PhysRevE.106.L022106](https://doi.org/10.1103/PhysRevE.106.L022106)

For the last three decades, small systems far from equilibrium, such as colloidal systems and organelles in cytoplasm, have been intensively studied owing to the advancement of theoretical development. The fluctuation theorems [1,2] and the Jarzynski [3] (or the Crooks [4]) work relation provide convenient means to compute the entropy production and free-energy change of the system. In addition, the stochastic thermodynamics [5,6] established the framework to calculate the thermodynamic quantities from the single-molecule trajectories. With the help of technical advances, these theories made it possible to investigate the long-standing thermodynamic questions, such as Maxwell's demon [7,8] and the Landauer's erasure bound [9,10]. In particular, much attention has been paid to the realization of stochastic heat engines. One type of simple engine consisting of a Brownian particle confined in a time-varying harmonic potential and temperature, is called a cyclic heat engine [11–14]. Another type is the steam engine in which a Brownian particle is periodically pushed by hot air bubbles created by a laser [15]. Steady-state autonomous engines have been also demonstrated, such as the Feynman-Smoluchowski ratchet [16] and the microrotator by demixing [17]. The efficiencies of autonomous engines were low, agreeing with the theoretical argument that autonomous engines cannot attain the Carnot efficiency [18,19], except in zero entropy production limit or in the injected heat divergent limit [20].

In recent years, a new thermodynamic principle called the thermodynamic uncertainty relation (TUR) [21–25], which provides the trade-off relation between thermodynamic fluctuations and cost, has been derived and experimentally confirmed [26–28]. The TUR in the steady state far from equilibrium is

$$\frac{\text{Var}[c(\tau)]}{\langle c(\tau) \rangle^2} \Delta S_{\text{tot}}(\tau) \geq 2k_B, \quad (1)$$

where k_B is the Boltzmann constant, c is a thermodynamics current, such as the work rate or the heat rate, and $\text{Var}(c) \equiv \langle (c - \langle c \rangle)^2 \rangle$ is the variance of the current. ΔS_{tot} is the mean total entropy production obtained from trajectories of duration τ . TUR implies a tighter bound than the thermodynamic second law ($\Delta S_{\text{tot}} \geq 0$). It has been applied to various systems, such as to deduce the efficiency bounds of steady-state heat engines [23,29], and biological motors [30,31], as well as to infer the entropy production rate without information on the potential or the force field [32–35].

In this Letter, we adopt the Brownian gyrotor to investigate the attainability of the Carnot efficiency of an autonomous heat engine. The linear Brownian gyrotor is a minimal model system for torque generation by extracting energy from thermal noises. It was conceptualized by Filliger *et al.* in a colloidal system [36], and has been theoretically studied [24,32,35,37–42] because it is an exactly solvable model. The engines have been realized experimentally in electric circuit systems [38] and colloidal systems [43], but without extracting work from the heat bath and thus not considered as a heat engine. By implementing appropriate parameters, we demonstrate that a Brownian gyrotor can work as an autonomous heat engine. For such a realization, we employ the optical feedback trap (OFT), which creates rapid well-controlled spatiotemporal potentials based on fast and accurate feedback loops to simultaneously apply conservative and nonconservative forces and artificial temperatures to the particles. We then confirm the efficiency of this autonomous linear engine can reach the Carnot limit. In addition, we show that TUR holds for the autonomous engine and as the engine efficiency approaches the Carnot efficiency, TUR converges to the lower bound.

Let us assume that the particle is immersed in water and confined by a symmetric two-dimensional harmonic potential with stiffness κ , $U(x, y) = (1/2)\kappa(x^2 + y^2)$, as shown by the yellow contour circles in Fig. 1(a). For the engine to extract energy from the heat bath, the particle is in contact with two different temperature baths, $T_x > T_y$, in the x and y axes (red and blue arrows). Additional nonconservative forces ($\epsilon_{x,y}$ and $\epsilon_{y,x}$ in the x and y directions, respectively) are applied to the

*pylai@phy.ncu.edu.tw

[†]yonggun@phy.ncu.edu.tw

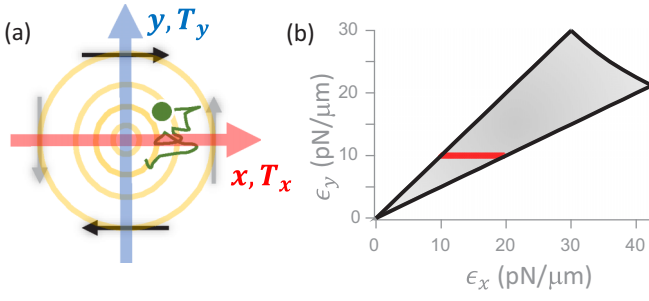


FIG. 1. (a) Schematic of the Brownian gyration. The particle (green circle) is under the symmetric harmonic potential (yellow circles) subject to the two temperature baths, $T_x > T_y$, and the given coupling forces, ϵ_{xy} (black arrow) and ϵ_{yx} (gray arrow). (b) The conditions of the region (gray) in which the gyration behaves as a linear heat engine. The red line represents the experimental values.

particle to transfer the heat from the hot bath to the cold bath. In this condition, the dynamics of the particle can be described by the overdamped Langevin equations as follows,

$$\gamma_x \dot{x} = -\kappa x + \epsilon_{xy} y + \xi_x(t), \quad (2)$$

$$\gamma_y \dot{y} = -\kappa y + \epsilon_{yx} x + \xi_y(t), \quad (3)$$

where γ_i is the friction coefficient, and i denotes x or y . The thermal random force $\langle \xi_i(t) \xi_j(t') \rangle = 2\gamma_i k_B T_i \delta_{ij} \delta(t - t')$, where δ_{ij} and $\delta(t - t')$ is the Kronecker delta and the Dirac delta function, respectively. Here, the total force acting on the particle is $\vec{F} = \vec{f}_c + \vec{f}_{nc}$, where $f_c^x = -\kappa x$ ($f_c^y = -\kappa y$) is the conservative force and $f_{nc}^x = \epsilon_{xy} y$ ($f_{nc}^y = \epsilon_{yx} x$) is the non-conservative force. To satisfy the stability condition that the conservative force has to trap the particle under the nonconservative force [37], the parameters of the system are constrained to be $\epsilon_y \leq \epsilon_x \leq (T_x/T_y)\epsilon_y$, and $\kappa^2 \geq \epsilon_x \epsilon_y$, which is represented by the gray shadow in Fig. 1(b) for $T_x/T_y = 2$.

The above linear heat engine is realized with a concurrent application of all the necessary forces using an optical feedback trap (OFT) [44,45]. The setup details are given in Sec. II of the Supplemental Material (SM) [46] and our previous work [14]. During the experiments, the stiffness of the harmonic potential is kept constant at $\kappa = 30$ pN/ μm . The medium temperature is at $T_R = 300$ K on both the x axis and the y axis. To create a difference in the effective temperatures, we applied an external random Gaussian force to the particle only in the x axis [14,47,48], and the effective temperature difference is set to be $\Delta T = 300$ K between the two axes such that $T_x = 600$ K. Here, we note that the medium viscosity is constant regardless of the effective temperature difference: $\gamma_x = \gamma_y = \gamma = 1.08$ mPa s. The coupling constant $\epsilon_y = 10$ pN/ μm is fixed while ϵ_x varies from 10 to 20 pN/ μm as depicted as the red line in Fig. 1(b).

Figures 2(a)–2(c) show the particle current map of $\vec{J}(x, y)$ superimposed on the nonequilibrium steady-state probability density $P_{ss}(x, y)$ of particle positions to aid visualization. The subscript “ss” denotes quantities under the nonequilibrium steady-state condition. The higher density of $P_{ss}(x, y)$ corresponds to the tilted darker regime in the grayscale color on

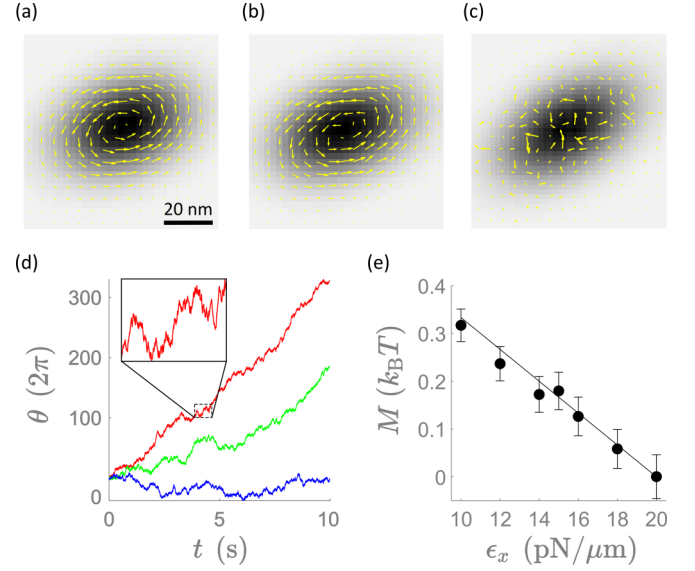


FIG. 2. (a)–(c) The steady-state probability density of particle positions $P_{ss}(\vec{x}, \vec{y})$ (grayscale) and the particle current map of $\vec{J}(x, y)$ (yellow arrows) for $\epsilon_x = 10, 15,$ and 20 pN/ μm at $\epsilon_y = 10$ pN/ μm , respectively. (d) Cumulative angular trajectories for $\epsilon_x = 10$ (red), 15 (green), and 20 (blue) pN/ μm . (e) The magnitude of the torque M for various ϵ_x . The error bars are the standard errors from 10^6 bootstrapped samples.

the map. The particle current $\vec{J}(x, y)$ is defined [43] as

$$\begin{bmatrix} J_x(x, y) \\ J_y(x, y) \end{bmatrix} = \begin{bmatrix} \langle x(t + \Delta t) - x(t) \rangle \\ \langle y(t + \Delta t) - y(t) \rangle \end{bmatrix}_{x(t)=x, y(t)=y} + \begin{bmatrix} \langle x(t) - x(t - \Delta t) \rangle \\ \langle y(t) - y(t - \Delta t) \rangle \end{bmatrix}_{x(t)=x, y(t)=y} \frac{P_{ss}(x, y)}{2\Delta t}, \quad (4)$$

where $\Delta t = 10^{-5}$ s is the inverse of the acquisition rate. $\vec{J}(x, y)$ is a counterclockwise rotating flow under the conditions of our experiments. The particle current is strongest at $\epsilon_x = \epsilon_y$, and gradually approaches to zero for $\epsilon_x = 2\epsilon_y$. We quantified it by calculating the accumulated revolutions of the rotational motion of the particles. Figure 2(d) shows the revolutions as a function of time for $\epsilon_x = 10, 15,$ and 20 pN/ μm , where the rotation angle is given by $\theta = \arctan(y/x)$. The stochastic nature of this engine is reflected in the fluctuations of the revolution [the inset of Fig. 2(d)].

The strength of the rotational motion can be computed in terms of the torque [36,43]. The magnitude of the torque is given by $M \equiv \langle |\vec{F} \times \vec{x}| \rangle = \langle |(\vec{f}_c + \vec{f}_{nc}) \times \vec{x}| \rangle$, and in the steady state can be calculated to be

$$M = \frac{k_B(\epsilon_y T_x - \epsilon_x T_y)}{\kappa}. \quad (5)$$

Figure 2(e) compares the measured M with the theoretical prediction.

We further examine the stochastic energetics of the autonomous linear heat engine. Due to the existence of the nonconservative force \vec{f}_{nc} , the linear engine stochastically transfers heat q_x from the hot bath to the cold one for useful work extraction ($-w$) as it gyrates. The energetics is calculated from the trajectory of a Brownian particle in the

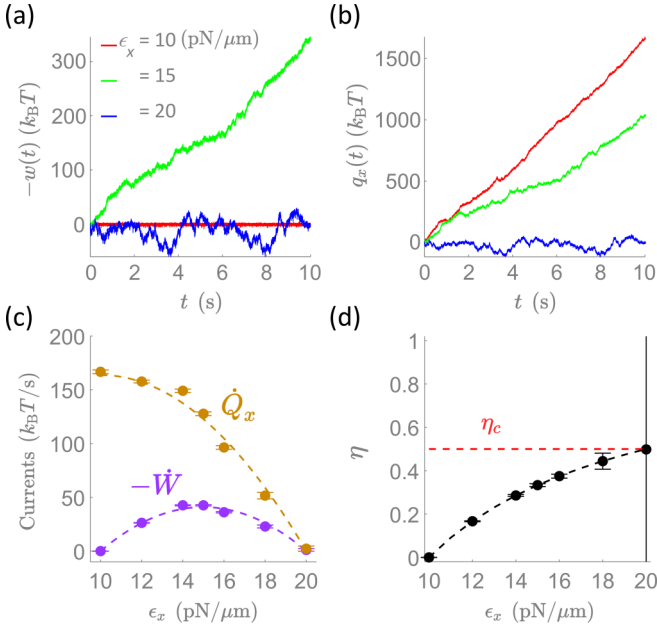


FIG. 3. The thermodynamic energetics of a linear engine. (a) The cumulative work output $-w(t)$ and (b) the cumulative heat to the particle $q_x(t)$ from the linear engine. (c) The mean work output rate $-\dot{W}$ and the mean heat rate \dot{Q}_x . The dashed curves are their respective theoretical predictions (8) and (9). Each rate is computed for 10 s and averaged. The error bars are the standard deviation of a bootstrapped sample with a size of 10^6 . (d) The efficiency of the linear engine (black solid circles). The error bars are the uncertainty calculated using error propagation from the standard deviation of both rates. The horizontal red dashed line denotes the Carnot efficiency η_c .

framework of stochastic thermodynamics [5,6]. The cumulative work and heat are defined respectively as

$$w(t) = \int_0^t \left[\left(\epsilon_x y \circ \frac{\partial x}{\partial s} + \epsilon_y x \circ \frac{\partial y}{\partial s} \right) ds \right], \quad (6)$$

$$q_x(t) = \int_0^t \left[\left(\kappa x - \epsilon_x y \right) \circ \frac{\partial x}{\partial s} \right] ds. \quad (7)$$

In the steady state, the work current (power output) can be obtained from a linear fitting of the cumulative work [Eq. (6)] or analytically derived to be (see Sec. III of SM) [49]

$$\begin{aligned} -\dot{W} &= -\epsilon_x \langle y \circ \dot{x} \rangle_{ss} - \epsilon_y \langle x \circ \dot{y} \rangle_{ss} \\ &= k_B \frac{(\epsilon_x - \epsilon_y)(T_x \epsilon_y - T_y \epsilon_x)}{2\kappa\gamma}, \end{aligned} \quad (8)$$

which is a quadratic function of ϵ_x for fixed ϵ_y . $-\dot{W}$ is zero at $\epsilon_x = \epsilon_y$, or $\epsilon_x = (T_x/T_y)\epsilon_y$, and has a maximum at $\epsilon_x^{\max} = \epsilon_y(1 + T_x/T_y)/2$. Similarly, the steady-state averages of the heat currents for hot and cold baths are as follows:

$$\dot{Q}_x = -\epsilon_x \langle y \circ \dot{x} \rangle_{ss} = k_B \frac{\epsilon_x(T_x \epsilon_y - T_y \epsilon_x)}{2\kappa\gamma}, \quad (9)$$

$$\dot{Q}_y = -\epsilon_y \langle x \circ \dot{y} \rangle_{ss} = -k_B \frac{\epsilon_y(T_x \epsilon_y - T_y \epsilon_x)}{2\kappa\gamma}. \quad (10)$$

Note that \dot{Q}_x decreases monotonically with ϵ_x .

Figures 3(a) and 3(b) plot the cumulative work $-w(t)$ and heat $q_x(t)$ of the engine for $\epsilon_x = 10$ pN/ μ m (red), 15 pN/ μ m

(green), and 20 pN/ μ m (blue) with a fixed $\epsilon_y = 10$ pN/ μ m, both showing a linear increase in time in the steady state within the explored range of ϵ_x . Figure 3(c) shows that the ensemble-averaged heat current from the hot bath \dot{Q}_x is maximum at $\epsilon_x = 10$ pN/ μ m, but with near-zero power ($\dot{W} \approx 0$). In contrast, a lower heat rate can bring about a larger output power and peak at $\epsilon_x = 1.5\epsilon_y = 15$ pN/ μ m. The ensemble averages of heat and work currents in our experiments agree well with the theoretical predictions.

The efficiency of the engine can be determined from the ratio of the work current $-\dot{W}$ to the injected heat current \dot{Q}_x : $\eta = -\dot{W}/\dot{Q}_x$. The steady-state efficiency can be obtained from Eqs. (8) and (9) to give

$$\eta = 1 - \frac{\epsilon_y}{\epsilon_x}. \quad (11)$$

Figure 3(d) shows that the efficiency agrees well with the theoretical prediction, which is expected since it depends only on ϵ_x and ϵ_y . For $\epsilon_x \rightarrow 2\epsilon_y$, η approaches the Carnot efficiency $\eta_c = 1/2$ while the power goes to zero, indicating the trade-off relation between these two quantities. The efficiency at maximum power can be directly calculated as $\eta_{MP} = 1 - \epsilon_y/\epsilon_x^{\max} = \eta_c/(2 - \eta_c)$, where $\eta_{MP} = 1/3$ at $\epsilon_x^{\max} = 1.5\epsilon_y$ in our engine. We note that $\eta_{MP} = \eta_c/2$ at $\eta_c \rightarrow 0$ since the thermodynamic fluxes are tightly coupled in this linear engine [50,51].

Next, we turn our attention to the TUR in Eq. (1), which can be rewritten as

$$\frac{D_X(\tau)}{\langle c(\tau) \rangle^2} \sigma(\tau) \geq k_B, \quad (12)$$

where $D_X(\tau) = \text{Var}[X(\tau)]/(2\tau)$ and X is a thermodynamic quantity such as work and heat. $c = \dot{X}$ is the current or the rate, and $\sigma = \Delta S_{\text{tot}}/\tau$ is the entropy production rate. For the autonomous linear engine, the exact relation between the thermodynamic variables and the control parameters can be analytically determined [23]. In the limit of $\tau \rightarrow \infty$, the direct calculation gives

$$\begin{aligned} \tilde{D} &\equiv \frac{D_w}{\dot{W}^2} = \frac{D_{q_x}}{\dot{Q}_x^2} = \frac{D_{q_y}}{\dot{Q}_y^2} \\ &= \frac{\gamma}{\kappa} \frac{[(\epsilon_x T_y - \epsilon_y T_x)^2 + 4\kappa^2 T_x T_y]}{(\epsilon_x T_y - \epsilon_y T_x)^2}, \end{aligned} \quad (13)$$

which is independent of duration τ . To measure $\text{Var}(X)$ experimentally, we acquired a single long trajectory lasting for at least 400 s and resampled it at a time interval of $\tau = 1$ s, which is 3000-fold larger than the relaxation time of the system, γ/κ . Therefore, a single long trajectory offers >400 steady-state samples to ensure robust statistics. Figure 4(a) shows 30 representative curves of the time-evolving work output $-w(t)$ (light purple) and the averaged value $\langle -w(t) \rangle = -W(t)$ (purple). The former is a fluctuating but increasing quantity in time while the latter accurately obeys a linear increase, which indicates the current $-\dot{W}$ is constant in time. The corresponding variance of $-w(t)$ is also a linearly increasing function and thus D_w is constant, confirming \tilde{D} is indeed time independent [Eq. (14)]. Figure 4(c) presents \tilde{D} (left axis) of the thermodynamic quantities against ϵ_x . We found that the \tilde{D} 's of \dot{W} ,

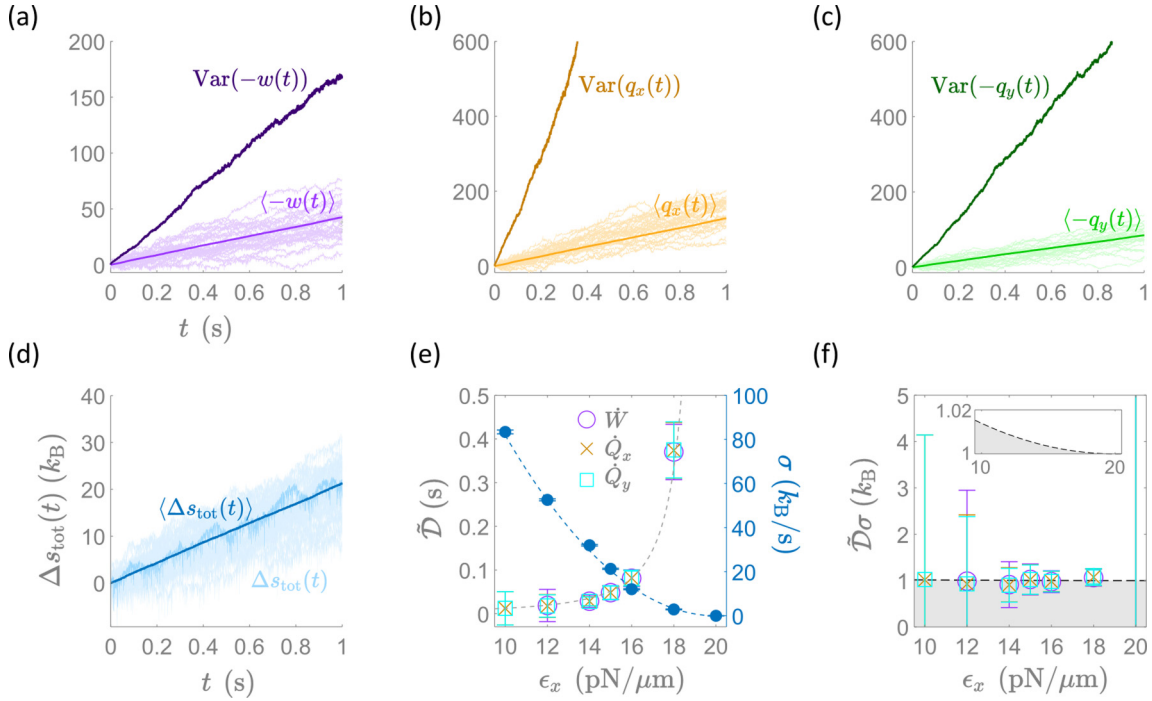


FIG. 4. (a) Thirty curves of work output $-w(t)$ (light purple), their time-evolved mean values $\langle -w(t) \rangle$ (purple), and variance $\text{Var}[-w(t)]$ (dark purple) are shown up to 1 s for $\epsilon_x = 15 \text{ pN}/\mu\text{m}$. The corresponding thermodynamic energetics $q_x(t)$ and $-q_y(t)$ are shown respectively in (b) and (c). The variance at each time point is determined from 500 samples. (d) The entropy production $\Delta s_{\text{tot}}(t)$ (light blue) and the averaged $\Delta S_{\text{tot}}(t)$ (blue). One $\Delta s_{\text{tot}}(t)$ curve is highlighted with medium blue color. (e) Left axis: \bar{D} of \dot{W} (open circle), \dot{Q}_x (cross), and \dot{Q}_y (open square). Right axis: The entropy production rate σ (solid circle). The dashed lines are the theoretical predictions. Error bars are root-mean-square errors derived from least-squares fits in (a)–(d). (f) The TUR of the currents. Note that at $\epsilon_x = 20 \text{ pN}/\mu\text{m}$, the caps of the error bar locate outside the range of interest. The gray shadow is the forbidden area. The black dashed (and the inset) line is the theoretical prediction [Eq. (17)] of the lower bound of TUR. The error bars are obtained from the error propagation.

\dot{Q}_x , and \dot{Q}_y all collapse into a single curve, agreeing with the theoretical prediction of Eq. (13) [23].

The total entropy production rate σ for the duration τ is $\sigma = \sigma_{\text{env}} + \sigma_{\text{sys}}$, where σ_{env} and σ_{sys} are the environment and system entropy production rates, respectively. For steady states with $\tau \rightarrow \infty$, only σ_{env} contributes to σ , and thus σ can be explicitly calculated from Eqs. (9) and (10) [40,49] to give

$$\sigma = \frac{\Delta S_{\text{tot}}}{\tau} = -\frac{\dot{Q}_x}{T_x} - \frac{\dot{Q}_y}{T_y} \quad (15)$$

$$= \frac{k_B}{2\kappa\gamma T_x T_y} (T_x \epsilon_y - T_y \epsilon_x)^2, \quad (16)$$

which is also constant in time. Figure 4(b) shows the measured total entropy production Δs_{tot} (light blue) of individual trajectories and their average ΔS_{tot} up to 1 s. As predicted, σ is constant in time, determined by the linear fitting. The results are shown in Fig. 4(c). As ϵ_x increases and approaches 20 $\text{pN}/\mu\text{m}$, σ asymptotically converges to zero since the engine approaches the reversible limit, well agreed with Eq. (16).

Finally, the TUR of the linear engine in a steady state can be examined by multiplying the measured σ with \bar{D} and

compared with the theoretical results using Eqs. (14) and (16):

$$\bar{D}\sigma = k_B \left[1 + \frac{(T_y \epsilon_x - T_x \epsilon_y)^2}{4\kappa^2 T_x T_y} \right] \geq k_B. \quad (17)$$

Figure 4(d) shows the measured $\bar{D}\sigma$ which is very close to the theoretical minimum of k_B in TUR, and TUR holds for this autonomous engine.

We demonstrated an autonomous linear heat engine of a single colloidal particle in contact with two heat reservoirs simultaneously and driven by a nonconservative coupling force. We confirmed that the linear engine obeys the TUR in the nonequilibrium steady state and also that TUR converges to the minimum when the engine efficiency approaches the Carnot efficiency. It is more challenging to study the dynamics of the Brownian gyrotor in contact with nonequilibrium noises with the persistence time [49], whose power and efficiency may surpass the Carnot efficiency.

This work has been supported by the Ministry of Science and Technology, Taiwan under Grants No. 110-2112-M-008-026-MY3 (P.Y.L.) and No. 110-2112-M-008-006- (Y.J.), and NCTS of Taiwan.

W.L. and Y.L. contributed equally to this work.

[1] U. Seifert, *Rep. Prog. Phys.* **75**, 126001 (2012).

[2] S. Ciliberto, *Phys. Rev. X* **7**, 021051 (2017).

[3] C. Jarzynski, *Phys. Rev. Lett.* **78**, 2690 (1997).

[4] G. E. Crooks, *Phys. Rev. E* **60**, 2721 (1999).

- [5] K. Sekimoto, *Prog. Theor. Phys. Suppl.* **130**, 17 (1998).
- [6] K. Sekimoto, *Stochastic Energetics* (Springer, Berlin, 2010), Vol. 799.
- [7] J. V. Koski, A. Kutvonen, I. M. Khaymovich, T. Ala-Nissila, and J. P. Pekola, *Phys. Rev. Lett.* **115**, 260602 (2015).
- [8] M. Ribezzi-Crivellari and F. Ritort, *Nat. Phys.* **15**, 660 (2019).
- [9] A. Bérut, A. Arakelyan, A. Petrosyan, S. Ciliberto, R. Dillenschneider, and E. Lutz, *Nature (London)* **483**, 187 (2012).
- [10] Y. Jun, M. Gavrilov, and J. Bechhoefer, *Phys. Rev. Lett.* **113**, 190601 (2014).
- [11] V. Blickle and C. Bechinger, *Nat. Phys.* **8**, 143 (2012).
- [12] I. A. Martínez, E. Roldán, L. Dinis, D. Petrov, J. M. R. Parrondo, and R. A. Rica, *Nat. Phys.* **12**, 67 (2016).
- [13] S. Krishnamurthy, S. Ghosh, D. Chatterji, R. Ganapathy, and A. K. Sood, *Nat. Phys.* **12**, 1134 (2016).
- [14] J. A. C. Albay, Z.-y. Zhou, C.-h. Chang, and Y. Jun, *Sci. Rep.* **11**, 4394 (2021).
- [15] P. A. Quinto-Su, *Nat. Commun.* **5**, 5889 (2014).
- [16] J. Bang, R. Pan, T. M. Hoang, J. Ahn, and C. Jarzynski, *New J. Phys.* **20**, 103032 (2018).
- [17] F. Schmidt, A. Magazzù, A. Callegari, L. Biancofiore, F. Cichos, and G. Volpe, *Phys. Rev. Lett.* **120**, 068004 (2018).
- [18] T. Hondou and K. Sekimoto, *Phys. Rev. E* **62**, 6021 (2000).
- [19] N. Shiraishi, *Phys. Rev. E* **92**, 050101(R) (2015).
- [20] J. S. Lee and H. Park, *Sci. Rep.* **7**, 10725 (2017).
- [21] A. C. Barato and U. Seifert, *Phys. Rev. Lett.* **114**, 158101 (2015).
- [22] T. R. Gingrich, J. M. Horowitz, N. Perunov, and J. L. England, *Phys. Rev. Lett.* **116**, 120601 (2016).
- [23] P. Pietzonka and U. Seifert, *Phys. Rev. Lett.* **120**, 190602 (2018).
- [24] J. Li, J. M. Horowitz, T. R. Gingrich, and N. Fakhri, *Nat. Commun.* **10**, 1666 (2019).
- [25] J. M. Horowitz and T. R. Gingrich, *Nat. Phys.* **16**, 15 (2020).
- [26] P. Pietzonka, F. Ritort, and U. Seifert, *Phys. Rev. E* **96**, 012101 (2017).
- [27] S. Pal, S. Saryal, D. Segal, T. S. Mahesh, and B. K. Agarwalla, *Phys. Rev. Research* **2**, 022044(R) (2020).
- [28] G. Paneru, S. Dutta, T. Tlusty, and H. K. Pak, *Phys. Rev. E* **102**, 032126 (2020).
- [29] V. Holubec and A. Ryabov, *Phys. Rev. Lett.* **121**, 120601 (2018).
- [30] P. Pietzonka, A. C. Barato, and U. Seifert, *J. Stat. Mech.: Theory Exp.* (2016) 124004.
- [31] Y. Song and C. Hyeon, *J. Chem. Phys.* **154**, 130901 (2021).
- [32] S. K. Manikandan, D. Gupta, and S. Krishnamurthy, *Phys. Rev. Lett.* **124**, 120603 (2020).
- [33] T. Van Vu, V. T. Vo, and Y. Hasegawa, *Phys. Rev. E* **101**, 042138 (2020).
- [34] S. Otsubo, S. Ito, A. Dechant, and T. Sagawa, *Phys. Rev. E* **101**, 062106 (2020).
- [35] S. K. Manikandan, S. Ghosh, A. Kundu, B. Das, V. Agrawal, D. Mitra, A. Banerjee, and S. Krishnamurthy, *Commun. Phys.* **4**, 258 (2021).
- [36] R. Filliger and P. Reimann, *Phys. Rev. Lett.* **99**, 230602 (2007).
- [37] J.-M. Park, H.-M. Chun, and J. D. Noh, *Phys. Rev. E* **94**, 012127 (2016).
- [38] K.-H. Chiang, C.-L. Lee, P.-Y. Lai, and Y.-F. Chen, *Phys. Rev. E* **96**, 032123 (2017).
- [39] S. K. Manikandan, L. Dabelow, R. Eichhorn, and S. Krishnamurthy, *Phys. Rev. Lett.* **122**, 140601 (2019).
- [40] D.-K. Kim, Y. Bae, S. Lee, and H. Jeong, *Phys. Rev. Lett.* **125**, 140604 (2020).
- [41] H. Chang, C.-L. Lee, P.-Y. Lai, and Y.-F. Chen, *Phys. Rev. E* **103**, 022128 (2021).
- [42] S. Otsubo, S. K. Manikandan, T. Sagawa, and S. Krishnamurthy, *Commun. Phys.* **5**, 11 (2022).
- [43] A. Argun, J. Soni, L. Dabelow, S. Bo, G. Pesce, R. Eichhorn, and G. Volpe, *Phys. Rev. E* **96**, 052106 (2017).
- [44] A. Kumar and J. Bechhoefer, *Appl. Phys. Lett.* **113**, 183702(2018).
- [45] J. A. C. Albay, G. Paneru, H. K. Pak, and Y. Jun, *Opt. Express* **26**, 29906 (2018).
- [46] See Supplemental Material at <http://link.aps.org/supplemental/10.1103/PhysRevE.106.L022106> for additional information.
- [47] P. Mestres, I. A. Martínez, A. Ortiz-Ambriz, R. A. Rica, and E. Roldan, *Phys. Rev. E* **90**, 032116 (2014).
- [48] I. A. Martínez, É. Roldán, J. M. R. Parrondo, and D. Petrov, *Phys. Rev. E* **87**, 032159 (2013).
- [49] J. S. Lee, J.-M. Park, and H. Park, *Phys. Rev. E* **102**, 032116 (2020).
- [50] C. Van den Broeck, *Phys. Rev. Lett.* **95**, 190602 (2005).
- [51] Z.-C. Tu, *Front. Phys.* **16**, 33202 (2021).